

Underfill Constraint Effects during Thermo-Mechanical Cycling of Flip Chip Solder Joints

I. Dutta, A. Gopinath and C. Marshall

Center for Materials Science and Engineering
Department of Mechanical Engineering
Naval Postgraduate School
Monterey, CA 93943.

Abstract

The presence of an 'underfill' encapsulant between a micro-electronic device and the underlying substrate is known to substantially improve the thermal fatigue life of flip-chip solder joints, primarily due to load-transfer from the solder to the encapsulant. In this study, a new single joint-shear (SJS) test, which allows the measurement of the strain response of an individual solder ball during thermo-mechanical cycling (TMC), has been utilized to investigate the impact of the constraint imposed by the underfill on a solder-joint. Finite element modeling has been utilized to demonstrate that the SJS sample geometry captures most of the deformation characteristics of a flip-chip joint, and to provide insight into the experimental observations. It has been shown that the strain response of a eutectic Pb-Sn solder joint is influenced significantly by *in-situ* microstructural coarsening during TMC, which in turn is dependent on the underfill properties. In general, underfill properties, which allowed the imposition of large compressive hydrostatic stresses on the solder joint, were the most effective in reducing coarsening. Phase coarsening prevented the stabilization of the stress-strain response of the solder even in the absence of crack-damage, and was found to depend strongly on the local inelastic strain state within the joint. This necessitates that future solder deformation models account for strain-history dependent microstructural evolution, and that underfill properties be optimized to minimize the extent of coarsening during TMC in order to maximize joint life.

1. Introduction

In flip chip (FC) technology, solder joints serve as both electrical and mechanical connections between a micro-electronic device and the substrate (or board). During typical service conditions, the electronic package undergoes thermal cycling, subjecting the solder joints to large cyclic shear strains due to the thermal expansion mismatch between the silicon chip and the polymer-based substrate. With increases in chip size and the density of input/output (I/O) connections, and decrease in joint size commensurate with reduction of the technology node size, solder joints are placed in ever-larger shear strains during service. The advent of underfill technology in the early 1990s alleviated this effect considerably [1], although solder life remains a significant source of concern with respect to package reliability.

The effect of filling the gap between the chip, substrate and the solder joints by a glass-filled epoxy underfill has been studied by numerous investigations [2-8]. The primary effect of the underfill is to reduce the shear load carried by the solder joints, thereby reducing the inelastic strain sustained by the solder and thus enhancing solder life. It has been shown [e.g., 3,8] that the presence of an underfill results in substantial redistribution of the displacement fields within a joint, and thereby reduces the extreme local strain concentrations which occur in joints without underfill. It is generally thought that stiff underfills with close CTE (coefficient of thermal expansion) match with solder are the most effective in enhancing package life.

Whereas it is well recognized that the deviatoric stress components, and hence the local inelastic strains, are mitigated by the underfill, its impact on the hydrostatic constraint imposed on the solder joints is less clear. As an example, Figure 1 shows the variation of the equivalent inelastic strain and hydrostatic stress (σ_{hyd}) with DNP (distance from the neutral point) along the joint mid-plane for a 5mm diagonal Si chip on FR-4 substrate at 298K, following underfill curing at 423K. The plane-strain model on which these calculations are based is also shown in the figure. While the joint inelastic strain expectedly increases with increasing DNP, it is also observed that σ_{hyd} for the outermost joints can reach large compressive values which are close to the yield strength of the Pb-Sn eutectic solder. Indeed, the actual σ_{hyd} is likely to be even greater, since 2-D models typically underestimate the hydrostatic constraint applied by the underfill on a solder ball. Still, because of computational expediency, most finite element (FE) models of flip-chip packages have been based on a 2-D approximation [e.g., 7], and even where 3-D models have been utilized [8,9], the role of the hydrostatic constraint *per se* has not been the subject of study.

While the mechanical effects of the 3-D constraints applied by the underfill on the solder joints can arguably be accounted for by appropriate modeling approaches, any microstructural effects that ensue because of these constraints (and the associated property changes) need to be studied by experimental means. To date, no study has reported on the role of underfill-related constraints on microstructural changes that occur in solder joints during thermo-mechanical cycling (TMC), although it is well known that local stress/strain states can have a significant impact on the solder microstructure during TMC [10]. As will be demonstrated in this paper, the constraint imposed by the underfill can have a significant impact on the microstructure, and hence the properties and reliability of a solder joint.

In this paper, we report on experimental measurements of the stress/strain response of model FC solder joints, with and without a surrounding underfill encapsulant, and correlate them with results of FE analysis, with the objective of providing insight into the interaction between the stress/strain field quantities and local microstructural effects within a solder joint.

2. Approach

2.1 Experimental

Nominally 2 mm diameter ball-shaped joints of Sn35Pb solder (simulating scaled-up FC joints) were utilized to join two 3mm diameter copper rods at their ends. Prior to joining, the joint-end of each rod was machined to simulate Cu bond pads of 1.6 mm diameter and 0.1mm thickness. Solder disks of 1.6 mm diameter and 1.4 mm thickness were produced by electric-discharge machining from a rolled solder plate of the same thickness. One such disk was placed between the fluxed bond-pads of two Cu rods, which were precisely aligned using an alignment fixture mounted on a screw-driven mechanical testing frame. The entire fixture was then heated to 488K, and the solder was reflowed for 2 minutes while adjusting the joint-gap to produce nominally 1.2 mm high, 2 mm diameter ball-shaped joints. The cooling rate following reflow was $\sim 20\text{K/minute}$.

For some of these samples, the space surrounding the solder between the two copper rods was filled with an underfill, thereby encapsulating the joint. This was accomplished by placing the as-joined sample in a closed Teflon™ fixture, and injecting the underfill through a hole in the fixture. In a few samples, a blow-hole was injected into the epoxy immediately following underfilling in order to simulate the effect of underfill voids. The Single Joint Shear (SJS) sample thus produced is schematically depicted in Figure 2, which also shows photographs of the non-underfilled and underfilled samples with and without voids.

Two different underfill materials supplied by Dexter Electronic Materials, HYSOL CNB 840-38™ and HYSOL FP 4549™, were selected for the present study. Labelled UF1 and UF2 respectively in this paper,

they had Young's moduli (E) of 11 GPa and 5.6 GPa, respectively, and coefficients of thermal expansion (CTE) of $21 \times 10^{-6}/\text{K}$ and $45 \times 10^{-6}/\text{K}$, respectively. For both underfills, the curing temperature was 428K.

Following sample preparation, an instrumented bi-metallic load-frame, utilizing the thermal expansion mismatch between Al and Invar, was used to impart temperature dependent shear displacements to the joints in the SJS specimen. The instrument, the design of which was adapted from ref. 11 with some modifications, utilizes several temperature compensated strain gauges, the outputs from which are used to compute continuous records of the applied force and shear displacement of the joint during thermal cycling. Each SJS specimen was subjected to 50 thermal cycles in Argon from 298K to 418K, with heating and cooling times of 15 minutes each, and dwell times of 10 minutes at the maximum and minimum temperatures. A schematic of the load-frame, along with photographs of the actual jig, are shown in Figure 3. The dimensions of the frame were such the solder joint was subjected to a nominal shear strain range of ~ 0.022 in the experimental temperature range, roughly simulating the loading conditions of a 200 μm diameter flip-chip solder joint between a Si chip and an FR-4TM board with a DNP (distance from the neutral point) of 2.5mm.

2.2 Numerical

Three-dimensional finite element (FE) models of the SJS sample, with and without underfill encapsulant, were constructed using ANSYSTM. For modeling expediency, the Cu rods were assumed to have a square cross section. All other dimensions of the experimental SJS sample were faithfully reproduced in the model. Because of the symmetry of the sample, only half of the sample was modeled, as shown in Figure 4. The Cu rods were modeled as thermo-elastic materials (since the load levels on Cu during SJS tests are too low to cause any permanent deformation), whereas the solder joint was modeled as a thermo-elastic-plastic-creeping solid with temperature dependent properties. The underfill materials were modeled as thermo-elastic, ignoring any viscoelastic effects. The solder/Cu, solder/underfill and underfill/Cu interfaces were all assumed to be perfectly adherent.

The solder was assumed to follow linear plasticity with a temperature dependent yield strength and work hardening rate, and display dislocation creep governed by a sinh law. The properties of the solder were gleaned from a combination of sources [12-14], and are listed in Table I. In addition to the underfills UF1 (high E, low CTE) and UF2 (low E, high CTE) which were utilized in the experiments, a third underfill UF3 (low E, low CTE) was also modeled, with the objective of deconvoluting the effects of underfill stiffness and thermal expansivity on solder strain response.

The model was meshed with 10-noded tetrahedral solid elements capable of sustaining large strain plasticity. Starting from an initial unstrained state at the underfill curing temperature (428K), the sample was first cooled to room temperature. Subsequently, the top and bottom halves of the sample were displaced relative to each other to produce a nominal joint shear strain of 0.02 over a temperature range of 298K to 418K. During cooling, the two halves were displaced back till to give zero nominal strain at 298K. This cycle was repeated several times to produce a stable stress-strain hysteresis loop for the solder joint.

3. **Results**

3.1 Numerical

Figure 5 shows a plot of the computed average shear stress at the solder / bond-pad interface during TMC, for samples with no underfill and with UF1, UF2 and UF3. For comparison, data from the 2-D flip chip (FC) model shown in Figure 1 are also plotted for an equivalent nominal shear strain range, starting from zero strain at room temperature. Given the similarity between the SJS and FC models, it is apparent that the SJS sample geometry captures the essential features of the FC joint behavior quite ably, and thus proffers a viable experimental approach to experimentally measure the response of a single flip chip joint.

Comparing the curves for the SJS samples with and without underfill, it is observed that (1) the range of stress hysteresis decreases due to the presence of the underfill encapsulant, (2) the stress range is smaller for larger underfill stiffness, and (3) the stress range decreases with increasing underfill CTE. Thus, the stress hysteresis is the largest for the joint without an encapsulant, and the smallest for UF1. UF2, the stiffness of which is about half that of UF1 (5.6GPa vs. 11 GPa, respectively), nevertheless results in only a slightly larger stress range. The effect of the lower E of UF2 is apparently mitigated by its larger CTE ($45 \times 10^{-6}/\text{K}$ vs. $21 \times 10^{-6}/\text{K}$ for UF2 and UF1, respectively), which, as will be shown later, allows UF2 to place the joint in significant hydrostatic compression, and thereby fosters a reduction in the interfacial shear stress. UF3, which has the same E as UF2, but possesses a smaller CTE ($21 \times 10^{-6}/\text{K}$), is the least effective in reducing the stress range, thereby demonstrating the efficacy of a high CTE value.

Similar effects are observed in the strain hysteresis curves shown in Figure 6. As in the case of stress, the FC and SJS models yield qualitatively very similar curves for interfacial shear strain hysteresis. The joint without an underfill encapsulant shows the largest strain range, with UF1 displaying the smallest, indicating the importance of underfills with high E. UF2 shows a larger strain range than UF1, with UF3 showing an even larger hysteresis. Thus a high E and a high CTE are both conducive to a smaller strain range, with E being the more effective.

Figures 7 and 8 show the distribution of hydrostatic stress and induced Von-Mises inelastic strain within the SJS solder joint at 298K and 405K, respectively. At 298K, which represents the low temperature end of the TMC with zero nominal joint shear strain ($\gamma_{\text{nom}}=0$), the middle of the joint is subjected to a small hydrostatic tension in the absence of an underfill ($\sim 5\text{MPa}$), and when the joint is encapsulated by UF1 ($\sim 8.5\text{MPa}$). This hydrostatic tension is associated with the constraint imposed by the copper pads on the shrinking solder during cooling. Since UF1 has a close CTE match with the solder, it provides little additional constraint. However, in the presence of UF2, which has a much larger CTE than solder, the middle of the joint is in large hydrostatic compression ($\sim -26\text{MPa}$). This hydrostatic compression is due to the relatively large shrinkage of UF2 surrounding the solder joint, which also results in a sufficient deviatoric stress to induce some inelastic strain in the solder at the lower temperatures. During subsequent heating, the small hydrostatic tension in the joints without underfill and with UF1 are rapidly relieved, as shown in Figure 8 at a temperature of 405K and $\gamma_{\text{nom}}=0.017$. Correspondingly, the applied shear displacement induces large inelastic strains within the joint. In the absence of an underfill, large inelastic strains are concentrated in bands running roughly parallel to the solder-bond pad interfaces. In the presence of an underfill encapsulant, however, the inelastic strains are more homogeneously distributed in the joint, and the near-interface strain concentrations are significantly reduced. This constitutes the primary impact of an underfill encapsulant around a solder joint.

When the joint is encapsulated by a high CTE underfill such as UF2, the large compressive hydrostatic stress present at 298K requires a larger temperature to get relieved completely, allowing a small compressive σ_{hyd} to be present even at 405K (Figure 8). It is also observed that the lower elastic modulus of UF2 relative to UF1 allows less inelastic strain redistribution (and hence less homogeneity in joint strain distribution), although the magnitude of the von-Mises inelastic strains induced in the middle of the joint during the heating segment of the TMC are comparable. However, it is noted that compared with the case without an underfill, both UF1 and UF2 result in significantly reduced inelastic strains near the solder / bond pad interface.

3.2 Experimental

Figure 9 shows the experimentally obtained plot of the average joint shear stress versus temperature during the 10th cycle. The experimental plots are qualitatively similar to the numerically obtained plots shown in Figure 5. Since the measurement starts with the joint in a stress-free state at ambient temperature (300K), the joint stress initially builds up elastically (linearly), till high temperature creep mechanisms start

operating. Beyond about 360K, the plot shows non-linearity with associated stress-relief due to creep. During cooling, stresses build up again, and at the very low temperature end, the joint yields plastically with large strain localization in shear bands, which allows the stress to return to a small value.

It is observed from Figure 9 that the stress range is the greatest for the joint without underfill, and the smallest for the joint with UF1. With defect-free UF2, the stress range is slightly larger than that with UF1, but when a blown-in defect is present in UF2, the stress range is considerably larger. These trends are similar to those observed numerically in that: (1) the underfill reduces nominal joint shear stress range in proportion to the underfill stiffness, and (2) a reduction in the constraint imposed by the underfill, e.g., due to the presence of a defect, increases the solder stress range.

Similar trends are observed for the average joint inelastic strain during the 10th cycle (Figure 10). As noted earlier, the observed inelastic strain hysteresis is due to the operation of creep and plastic yielding. While heating from the ambient, no inelastic strain is induced initially as the joint is loaded elastically, following which high temperature creep mechanisms become operational. The creep strains increase rapidly, and during cooling, steadily decrease to a near-zero value. The strain range is the largest for the joint without the underfill, and smallest for the joint with UF1. It is slightly larger for UF2 than for UF1 (due to the smaller E of UF2), and even larger when there is a defect in UF2. The defect allows the hydrostatic constraint applied on the solder by the underfill to be partially relaxed, thereby allowing strain range to increase.

Figure 11 plots the average joint inelastic strain range per cycle ($\Delta\gamma_{inel}$) as a function of the number of elapsed cycles (N). As noted above, $\Delta\gamma_{inel}$ starts out being the largest for the joint without underfill, and the smallest for the joint with defect-free UF1, with defect-free UF2 and defected UF2 being in between. However, unlike in the numerical calculations, where stable strain hysteresis conditions were established after the first 3-5 cycles, the experimental $\Delta\gamma_{inel}$ is observed to steadily increase in magnitude with progressive cycling.

It is further observed that the rate of increase of $\Delta\gamma_{inel}$ with N is the greatest for the joint without underfill, and least for the joint with defect-free UF2. Indeed, while the presence of an underfill invariably reduces the slope of the $\Delta\gamma_{inel}$ vs. N plot, the presence of a defect-free, high CTE underfill (e.g., UF2) appears to have the greatest impact, resulting in strain-range saturation (i.e., a stable strain hysteresis) after about 25 cycles. Introduction of a defect in the underfill, however, relaxes the hydrostatic constraint on the solder joint, and results in an increase in the slope. Clearly, therefore, whereas the magnitude of $\Delta\gamma_{inel}$ at the beginning of cycling is related to both E and CTE of the underfill, the slope of the $\Delta\gamma_{inel}$ vs. N plot is largely dependent on the underfill CTE, and hence the applied hydrostatic constraint.

Microstructural examination of the as-tested samples failed to reveal any evidence of damage via crack nucleation at the joint/bond-pad interface or within the joints themselves after 50 cycles. However, a distinct difference in the microstructural scale within the joints was noted after cycling, although the starting microstructures were very similar. This is apparent from Figure 12, which shows the microstructures within the solder joints with and without underfill slightly away from the bond-pad / solder interface, before and after thermal cycling. It is clear that in the absence of underfill, the solder microstructure coarsens very significantly, with a general spheroidization of the Pb-rich phase, within the 50 thermal cycles to which the joint was subjected. Similar locations within the joints with underfill show less coarsening and spheroidization, the joint with UF1 showing greater coarsening than the joint with UF2. It is this microstructural coarsening during TMC that is responsible for the increase in the magnitude of $\Delta\gamma_{inel}$ with increasing N, as noted in Figure 11.

Figure 13 shows that the extent of microstructural coarsening within a solder joint (without underfill) varies considerably depending on location. Following TMC, it is possible to correlate the local microstructural scale within the joint with the local accumulated inelastic strain. It is apparent from the

figure that the microstructure within the joint is very inhomogeneous, with the extent of coarsening appearing to increase with increasing cumulative strain, as computed numerically. The regions near the side-walls of the joint, where the cumulative strain is the least, retain the original microstructural scale after 50 cycles, whereas the region near the interface with the bond-pad, where the strains are high, show the maximum amount of coarsening. In contrast to the joint without underfill, for joints encapsulated by an underfill (either UF1 or UF2), the microstructure throughout the joint was observed to be relatively uniform, indicating that the internal strain distributions in these samples were much less inhomogeneous.

3. Discussion

The above results suggest that the extent of phase coarsening during thermo-mechanical cycling of solder joints is at least partly dependent on the local inelastic strain state. It is also apparent that the extent of coarsening is strongly dependent on whether or not an underfill encapsulant is present, as well as the properties of the underfill. Clearly then, the constraint applied by the underfill on the joint is of importance.

As noted in Figure 7, following initial cooling to 298K after initial re-flow, the joint with UF2 is placed under significant hydrostatic compression, whereas the joint with UF1 and that without an underfill are observed to be under small tension (5-8MPa). The hydrostatic compression in the joint with UF2 arises from the much larger CTE of the underfill relative to that of the solder, and suppresses plastic deformation during subsequent heating. Following heating to 405K (Figure 8), for instance, the magnitudes of the hydrostatic stresses in all the joints decrease substantially, but whereas $\sigma_{\text{hyd}} \sim 0$ for the joints without underfill and with UF1, the joint with UF2 is still under a small hydrostatic compression. Thus the hydrostatic stress in the joint with UF2, being initially larger in magnitude, requires a larger temperature range to be relieved, and is thus able to reduce the inelastic strains induced during thermal cycling following initial cooling from the reflow temperature. Additionally, depending on their magnitude, the compressive hydrostatic stresses may also inhibit phase coarsening by reducing local vacancy concentration and hence diffusive fluxes within the joint.

In turn, the reduction of plasticity reduces the rate of phase coarsening, as suggested by Figures 12 and 13. Since the progressive increase in the magnitude of $\Delta\gamma_{\text{inel}}$ with increasing number of thermo-mechanical cycles, as noted in Figure 11, is attributable to the extent of *in-situ* phase coarsening, inhibition of coarsening is expected to result in a stable strain response during TMC (i.e., where the strain range $\Delta\gamma_{\text{inel}}$ does not increase with N), as observed for UF2. Thus, an underfill applying a large compressive hydrostatic constraint on the deforming solder joint seems best able to produce a stable thermal cycling response prior to crack initiation in the joint. Contrarily, in a joint without underfill, or when the underfill applies little constraint on the joint, the inelastic strain range slowly increases with progressive cycling, never reaching saturation. Relaxation of the constraint applied by the underfill on the solder joint due to the presence of defects was observed to result in a greater rate of increase of $\Delta\gamma_{\text{inel}}$ with N, reinforcing the notion that a larger constraint is more favorable.

Whereas the hydrostatic constraint due to the underfill has an indirect effect on the inelastic strain range via its effect on microstructural coarsening, underfill stiffness has a direct impact. As expected, increased underfill stiffness reduces stresses and inelastic strain levels in the solder in proportion to E_{uf} . Additionally, a higher E_{uf} results in a more homogeneous internal strain distribution within each joint, and this is reflected by the spatial uniformity of the microstructures observed in the joints with underfill after TMC, in contrast to the microstructural inhomogeneity of the joint without underfill. Clearly therefore, the ideal underfill would be stiff, and yet able to apply a significant compressive constraint on the solder joints. Unfortunately, a very large CTE, such as that of UF2, is not suitable for a real package, since it would cause unacceptable shear distortion of the package as a whole, as well as of the solder joints situated at

large DNP. However, an underfill CTE slightly larger than that of the solder, in conjunction with a high E_{uf} , would appear to be very effective in enhancing solder life.

The present study clearly demonstrates that the underfill properties have a strong influence on not only the nominal inelastic strain range which the joint is subjected to, but also on the evolution of the inelastic strain range with continued cycling due to the ensuing microstructural changes. It also demonstrates that the microstructural changes occurring during TMC are related both to the prior plastic strain history of the joint, as well as the hydrostatic constraint to which the joint is subjected. Therefore, it is imperative that these microstructural changes be accounted for in methodologies utilized for life-prediction of solders. This suggests that it is necessary to develop new constitutive creep laws, explicitly accounting for simultaneous, hydrostatic-stress-state and plastic-strain-history dependent phase coarsening, and incorporate these laws into life-prediction models.

4. Conclusions

A new single-joint-shear (SJS) approach was used to measure the nominal stress/strain response of a single solder ball joint during thermo-mechanical cycling. Numerical simulations showed that for the most part, the SJS sample geometry captures the deformation characteristics of a flip-chip or BGA joint, and therefore provides a convenient means of quantitatively studying the behavior of a real microelectronic solder joint.

It was shown that the presence of an underfill reduces the stress and inelastic strain levels on flip-chip solder joints in proportion to the underfill stiffness. The hydrostatic constraint on the solder joint, which is strongly dependent on the CTE mismatch between the solder and underfill, was also shown to have a significant effect. It was shown that without underfill, microstructural coarsening in a eutectic lead-tin solder may be significant, even in 50 cycles. The extent of coarsening was found to vary significantly with location within a joint, and was related to the local inelastic strain state. The coarsening kinetics were slowed appreciably in the presence of an underfill, with increasing underfill stiffness and CTE having greater impact. Whereas a stiffer underfill was known to be of advantage, the observed beneficial effect of a high underfill CTE, was not anticipated *a priori*. It was found that this effect is due to the inhibition of *in-situ* phase coarsening within the solder joint by underfills of high CTE, and may be attributed to the increased compressive hydrostatic constraint they are able to apply on a solder joint. The presence of hydrostatic compression reduced phase coarsening kinetics, primarily by reducing the cumulative inelastic strains stored in the solder, although secondary effects due to depression of vacancy concentrations (and hence diffusive fluxes) may also play a role. The presence of defects in the underfill reduced its beneficial effects by lowering the hydrostatic constraint and the extent of the applied load supported by the underfill. Importantly, the results of this work establish the need for developing new constitutive deformation laws for solders, accounting for local stress/strain-state dependent microstructural coarsening, so that more reliable life-prediction models may be formulated in the future.

Acknowledgements

The authors are grateful to Dexter Electronic Materials for making the underfill materials and related information available for this work. The authors are thankful to Mr. Tom Christian for his assistance with the experimental set-up. ID also acknowledges several valuable discussions with Drs. Darrel Frear and Vijay Sarihan of Motorola. The work was supported by the Research Office of the Naval Postgraduate School through the NIFR program.

References :

1. D. Suryanarayana, R. Hsiao, T. P. Gall and J. M. McCreary, "Enhancement of Flip-Chip Fatigue Life by Encapsulation", IEEE Trans. CHMT, 14, 1991, pp. 218-223.
2. Y. Tsukada, Y. Mashimoto, T. Nishio and N. Mii, "Reliability and Stress Analysis of Encapsulated Flip Chip Joint on Epoxy Base Printed Circuit Board", Proc. 1st ASME/JSME Advances in Electronic Packaging Conf., 1992, pp. 827-835.
3. Y. Guo, W.T. Chen and K.C. Lim, "Experimental Determinations of Thermal Strains in Semiconductor Packaging using Moire Interferometry", Proc. 1st ASME/JSME Advances in Electronic Packaging Conf., 1992, pp. 779-784.
4. J. H. Lau, T. Krulevitch, W. Schar, M. Heydinger, S. Erasmus and J. Gleason, "Experimental and Analytical Studies of Encapsulated Flip Chip Solder Bumps on Surface Laminar Circuit Boards", Circuit World, 19, 1993, pp. 18-24.
5. C.P. Wong, J. M. Segelken and C.N. Robinson, "Chip on Board Encapsulation", in Chip on Board Technologies for Multi-Chip Modules, J. H. Lau, ed., Van Nostrand Reinhold, New York, NY, 1994, pp. 470-503.
6. J. H. Lau, "Solder Joint Reliability of Flip Chip and Plastic Ball Grid Array Assemblies Under Thermal, Mechanical and Vibration Conditions", IEEE Trans. CHMT, Part B, 19, 1996, pp. 728-735.
7. J. H. Lau, S-W. R. Lee, C. Chang and C. Ouyang, "Effects of Underfill Material Properties on the Reliability of Solder Bumped Flip Chip on Board with Underfill Encapsulants", Proc. IEEE ECTC , 1999, pp. 571-581.
8. P. Su, S. Rzepka, M. Korhonen and C.Y. Li, "The Effects of Underfill on the Reliability of Flip Chip Solder Joints", J. Electronic Mater., 28, 1999, pp. 1017-1022.
9. A. Schubert, R. Dudek, J. Kloser, B. Michel, H. Reichl, R. Hauck and K. Kaskoun, "Experimental and Numerical Reliability Investigations of FCOB Assemblies with Process-induced Defects", Proc. IEEE ECTC, 2000, pp.624-632.
10. J. W. Morris, J. L. Freer Goldstein and Z. Mei, "Microstructural Influences on the Mechanical Properties of Solder", in The Mechanics of Solder Alloy Interconnects, D.R. Frear, S.N. Burchett, H.S. Morgan and J.H. Lau, eds., Van Nostrand Reinhold, 1994, pp. 7-41.
11. P.L. Hacke, A.F. Sprecher and H. Conrad, "Modeling of the Thermo-mechanical Fatigue of 63Sn-37Pb Alloy", in Thermomechanical Fatigue Behavior of Materials, ASTM STP 1186, ASTM, Philadelphia, 1993, pp. 91-105.
12. Metals Handbook, Vol. 2, ASM International, 10th Edition, 1990, pp. 543-556.
13. C.E. Hanna, S. Michaelides, P. Palaniappan, D.F. Baldwin and S.K. Sitaraman, "Numerical and Experimental Study of the Evolution of Stresses in Flip Chip Assemblies During Assembly and Thermal Cycling", Proc. IEEE ECTC, 1999, pp. 1001-1009.
14. J.J. Stephens and D. R. Frear, "Time-Dependent Deformation Behavior of Near-Eutectic 60Sn-40Pb Solder", Metall. Mater. Trans. A, 30A, 1999, pp. 1301-1313.

TABLE I : Solder Properties Used in FE Model

Elastic Properties:

Temperature (K)	Young' Modulus (GPa)	Poisson's Ratio
423	18.8	0.4
398	21	0.4
373	23.2	0.4
348	25.4	0.4
323	27.6	0.4
298	29.8	0.4

Bilinear Isotropic Plastic Properties:

Temperature (K)	Yield Strength (MPa)	Tangent Modulus (MPa)
423	7.5	173
398	10.8	178
373	14	184
348	17.4	189
323	20.7	194
298	24	200

Creep Equation:

$$\dot{\epsilon} = 2.48 \times 10^4 \left[\sinh(0.0793 \sigma(\text{MPa})) \right]^{3.04} \exp \left[-\frac{56,994 \text{ J / mole}}{RT} \right]$$

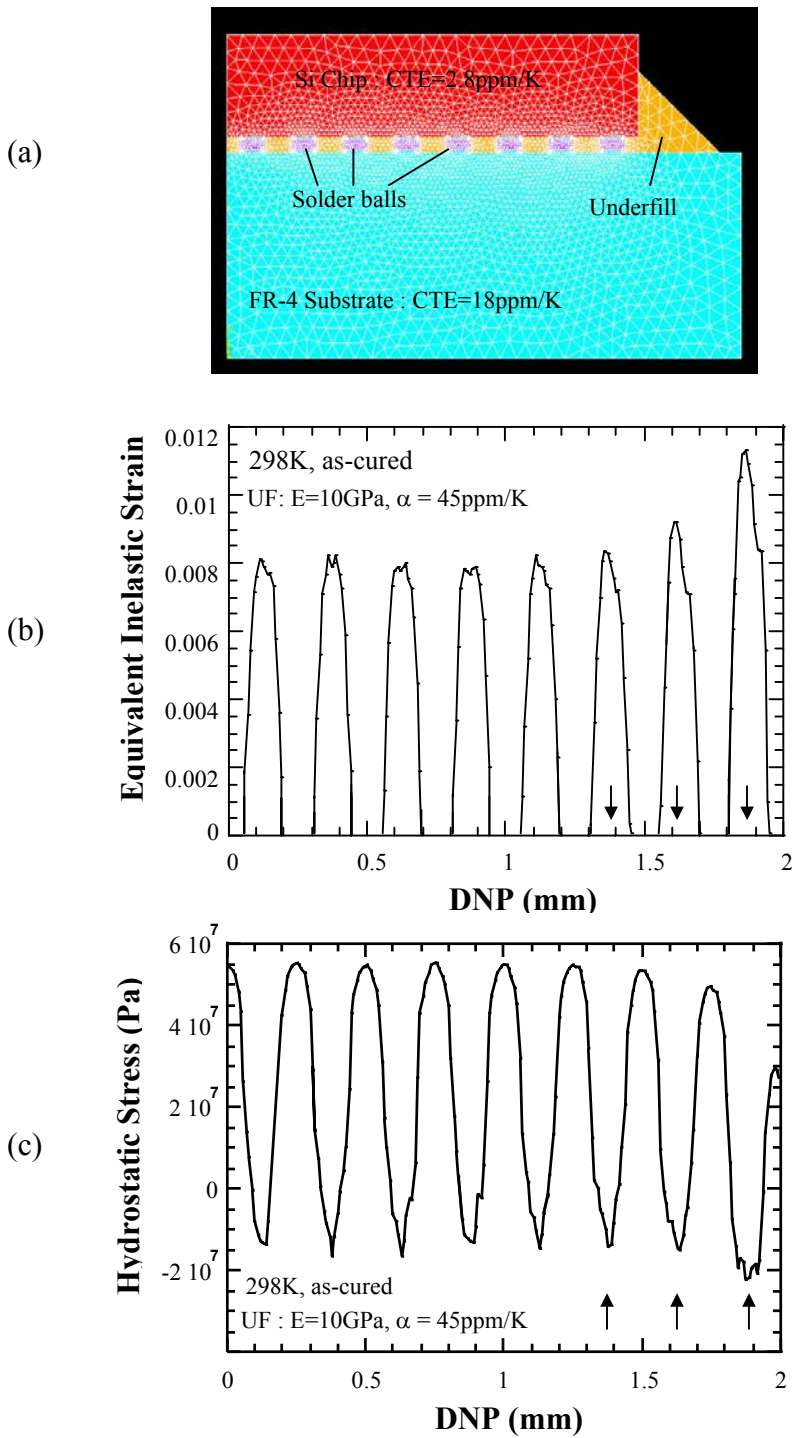


Figure 1: 2-D plane strain FE model of a flip-chip package (a), and the computed variation of (b) equivalent inelastic strain and (c) hydrostatic stress along the mid-plane of the solder balls with DNP. The locations of the 3 outermost solder joints is indicated by arrows. The inelastic strain in the solder joint increases with increasing DNP, but the outermost solder joint is also subjected to large hydrostatic stress (~ 20 MPa).

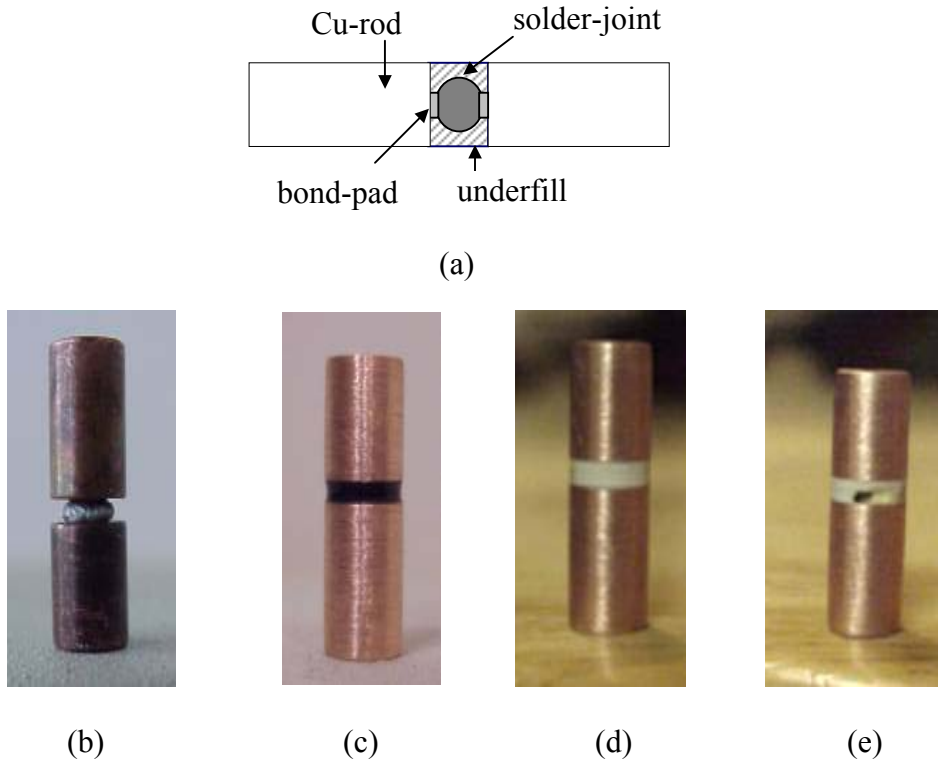


Figure 2: (a) Schematic of the SJS sample, showing the solder ball located between two copper rods, surrounded by an underfill encapsulant. (b-e) Photographs of SJS samples without underfill, with UF1, with UF2, and with UF2 containing a blown-in defect, respectively.

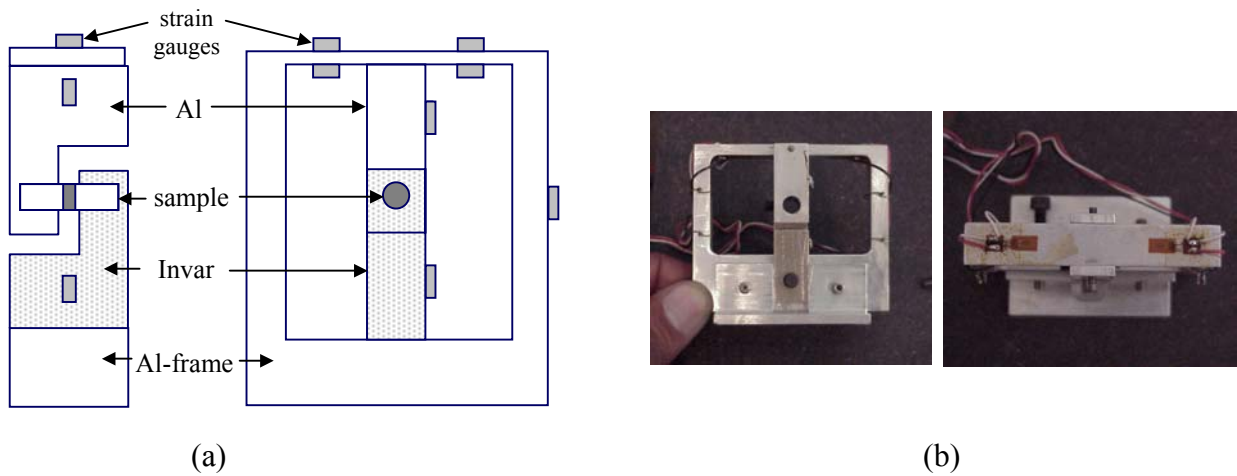


Figure 3 : (a) Schematic of the side and front elevations of the instrumented SJS test frame, showing the sample mounted between Al and Invar grips, which are attached to an Al-frame. (b) Photographs of the front and top views of the actual test frame.

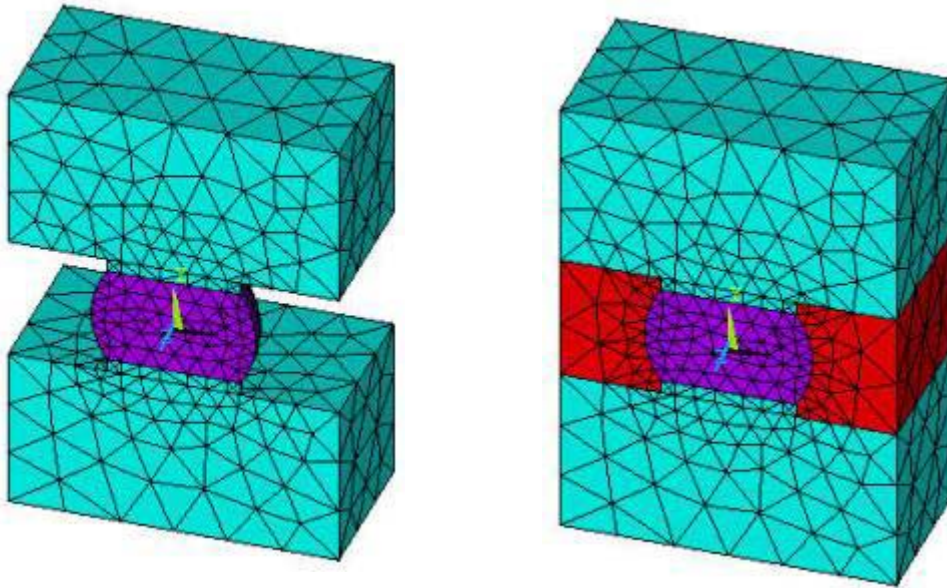


Figure 4 : Three-dimensional FE models of the SJS samples without and with an underfill encapsulant.

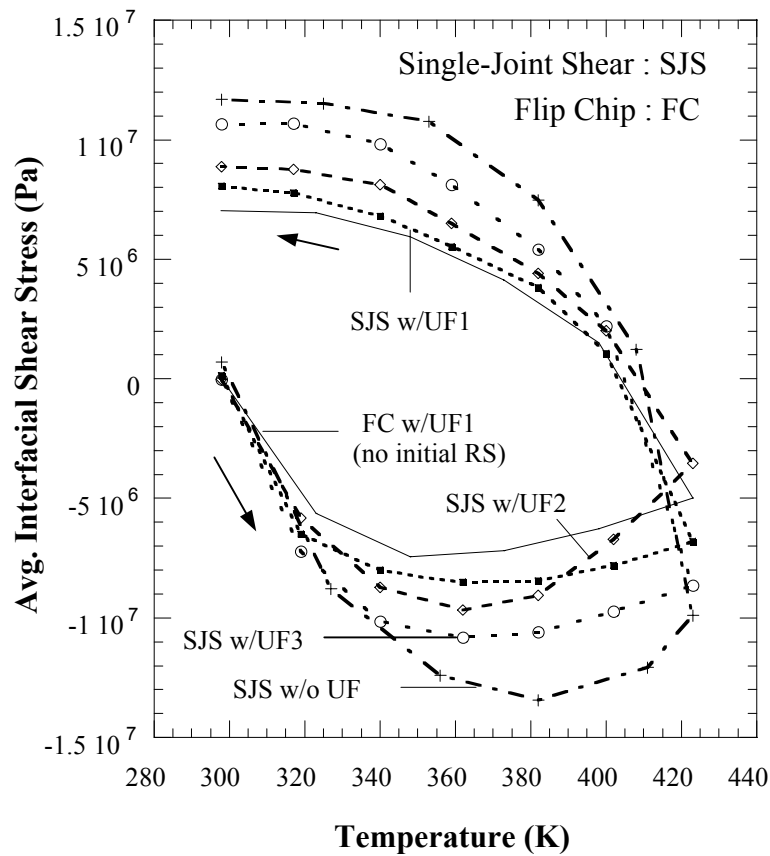


Figure 5: Computed variation of the average shear stress at the solder/bond-pad interface with temperature during TMC. Plots for SJS samples without and with various underfills are shown. For comparison, results from the 2-D plane strain FC model of Figure 1, assuming that room temperature corresponds to a state of zero imposed strain, are also shown.

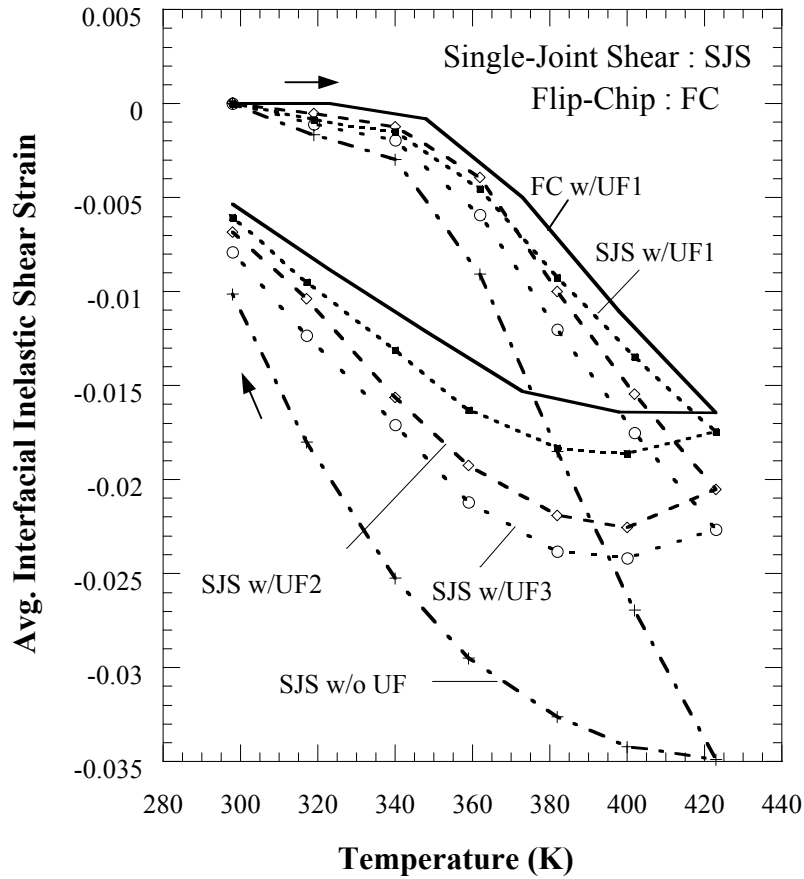


Figure 6: Computed variation of the average shear strain at the solder/bond-pad interface with temperature during TMC. Plots for SJS samples without and with various underfills are shown. For comparison, results from the 2-D plane strain FC model of Figure 1, assuming that room temperature corresponds to a state of zero imposed strain, are also shown.

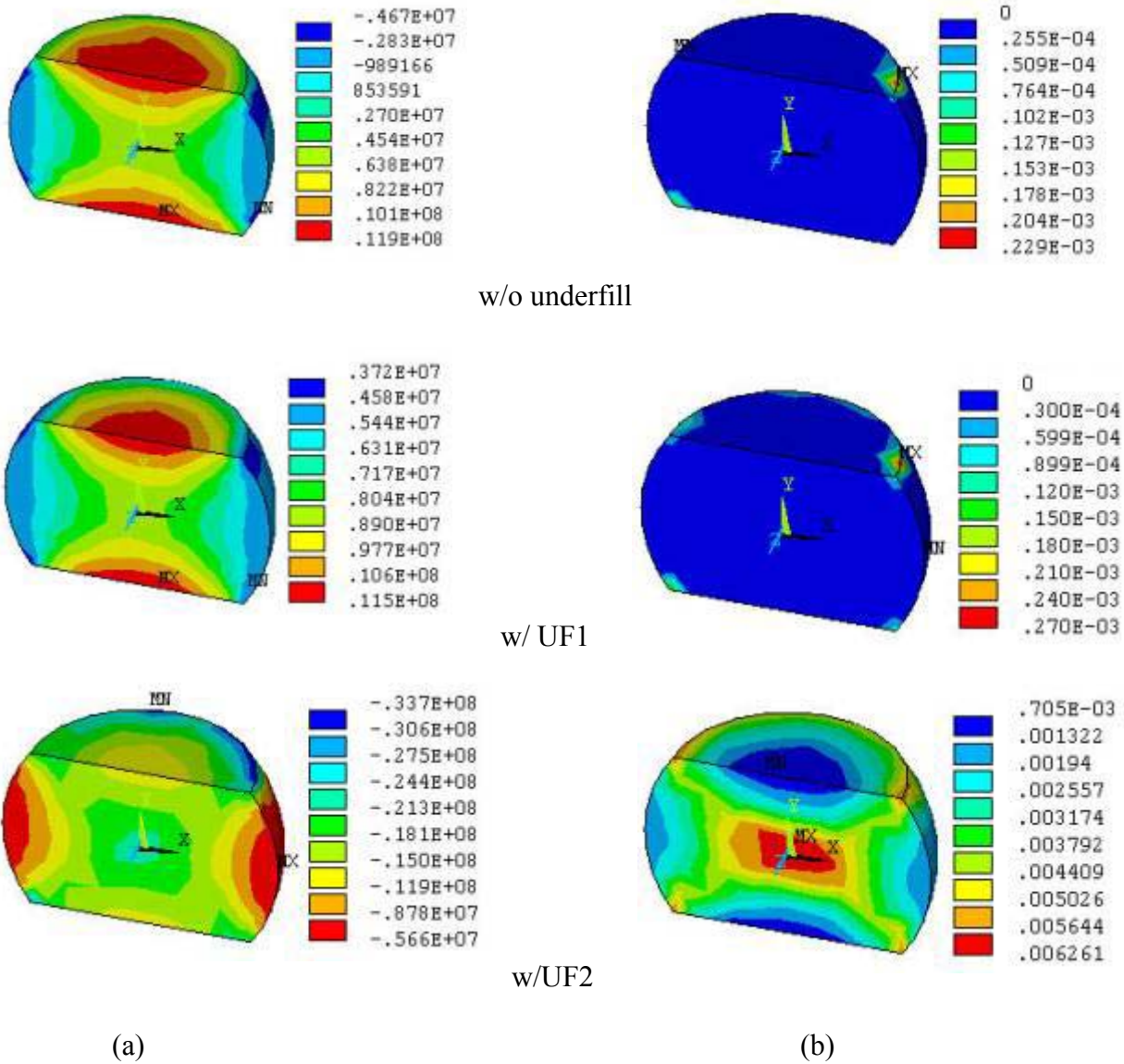


Figure 7 : Distribution of (a) hydrostatic stress, and (b) von-Mises inelastic strain in the SJS solder ball at 298K, following initial cooling from the reflow temperature. Large compressive hydrostatic stresses are observed to be present in the middle of the joint encapsulated by UF2. Whereas the joints without underfill and with UF1 show no inelastic strain, a small inelastic strain is induced in the joint with UF2 because of the large underfill CTE.

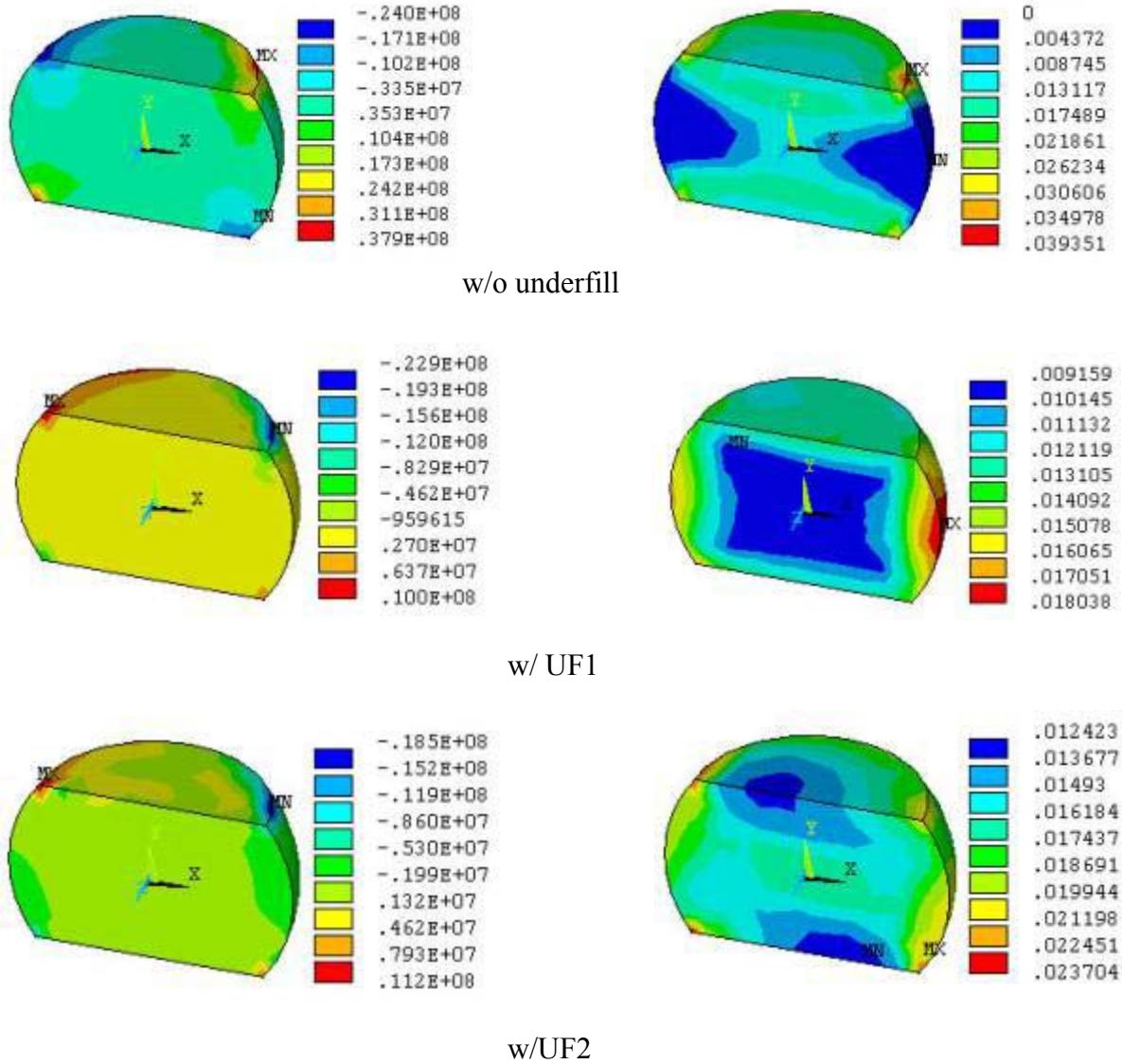


Figure 8: Distribution of (a) hydrostatic stress, and (b) cumulative von-Mises inelastic strain in the SJS solder ball after heating to 405K. This temperature corresponds to a nominal applied shear strain of 0.017. The hydrostatic stresses are largely relieved, but whereas the middle of the joints without underfill and with UF1 are in slight tension, the middle of the joint with UF2 is still under slight compression. The inelastic strain in the joint without underfill is concentrated in bands parallel to the joint/bond-pad interface. In the joints with underfill, smaller inelastic strains are induced in the regions near the interface during heating from 298K to 405K.

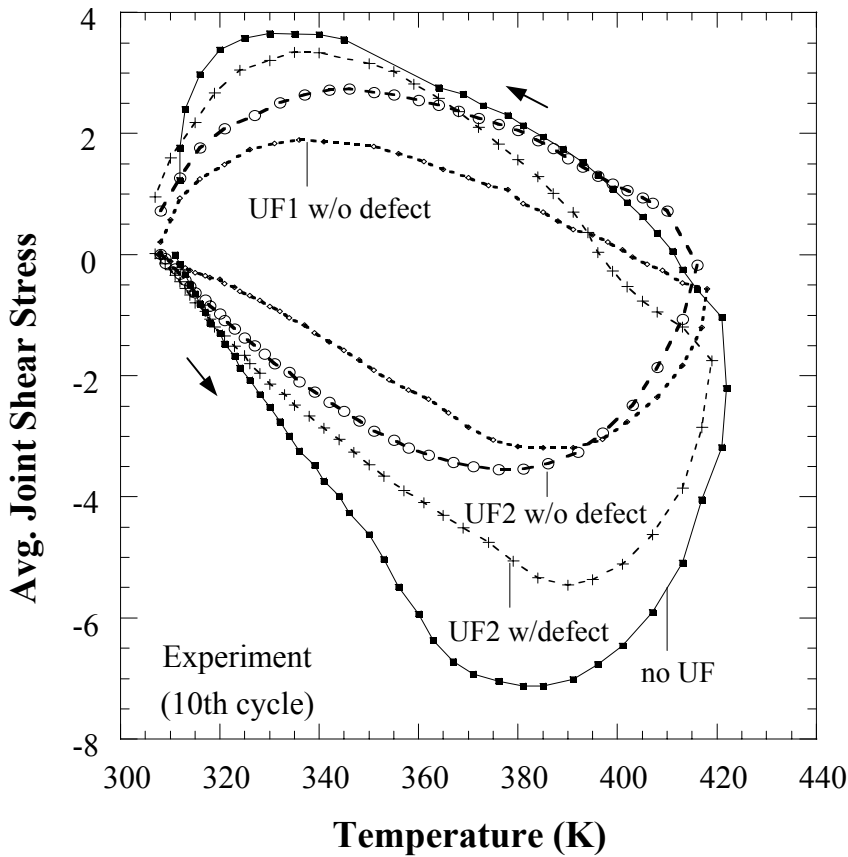


Figure 9: Plot of the experimentally measured average joint shear stress as a function of thermal cycling temperature during the 10th cycle. The underfill is observed to have a strong effect on the behavior of the SJS sample.

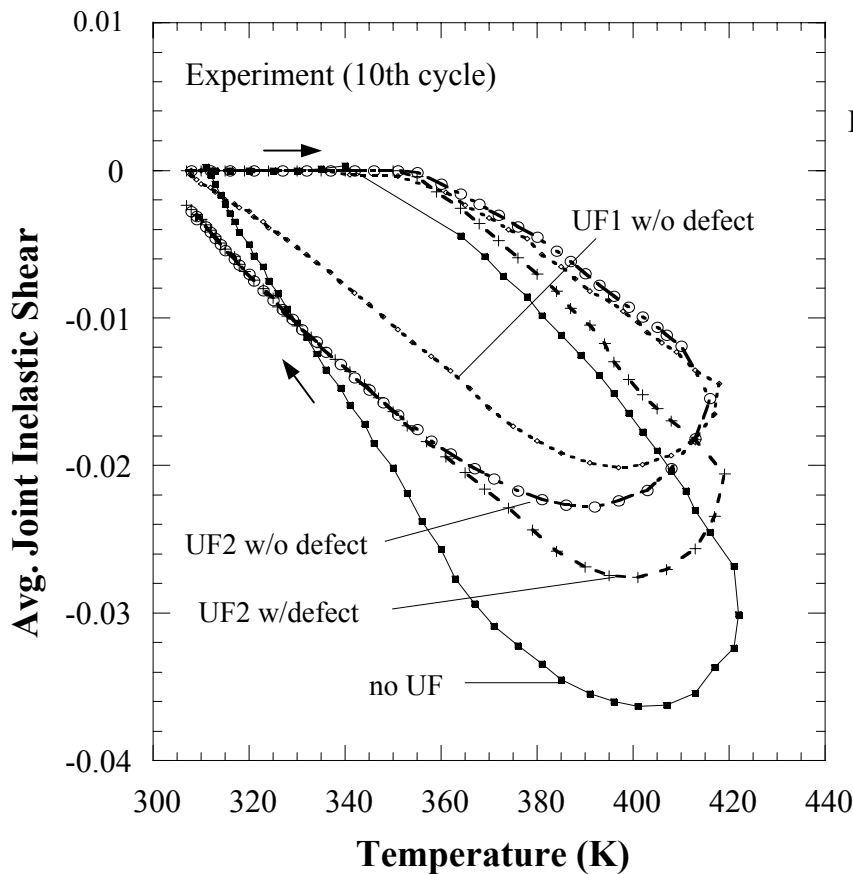


Figure 10: Plot of the experimentally measured average joint inelastic strain as a function of thermal cycling temperature during the 10th cycle. The inelastic strain range to which the joint is subjected is strongly affected by the underfill properties.

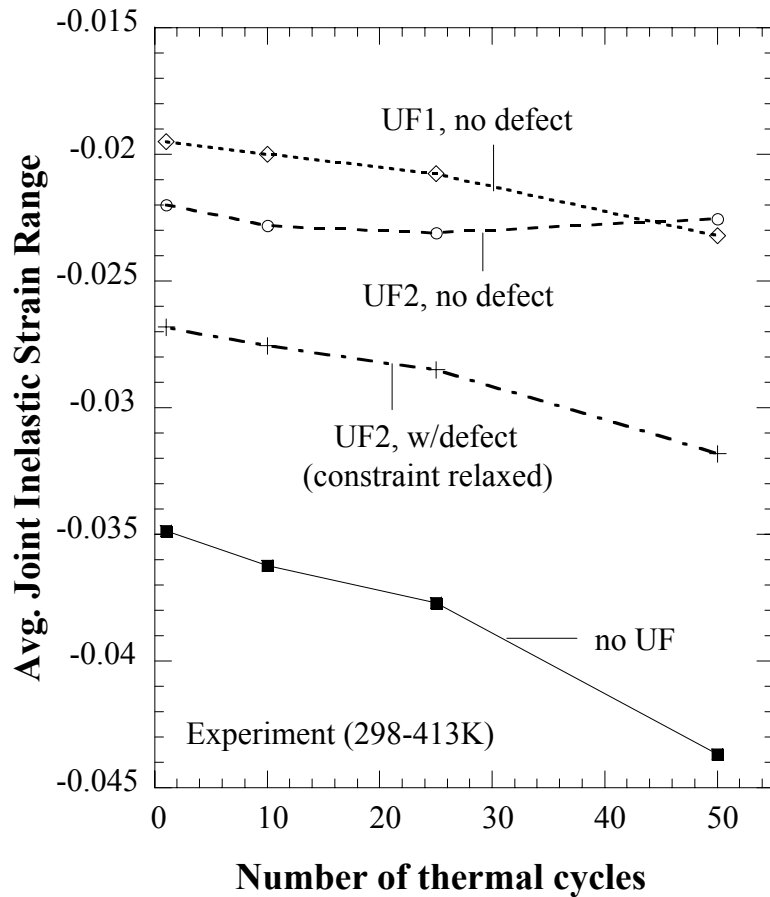


Figure 11: Plot of the experimentally measured average joint inelastic strain range ($\Delta\gamma_{inel}$) against the number of elapsed thermo-mechanical cycles (N). The magnitude of $\Delta\gamma_{inel}$ is observed to increase with N, even when there is no crack-damage. The rate of increase of $\Delta\gamma_{inel}$ with N depends strongly on underfill characteristics.

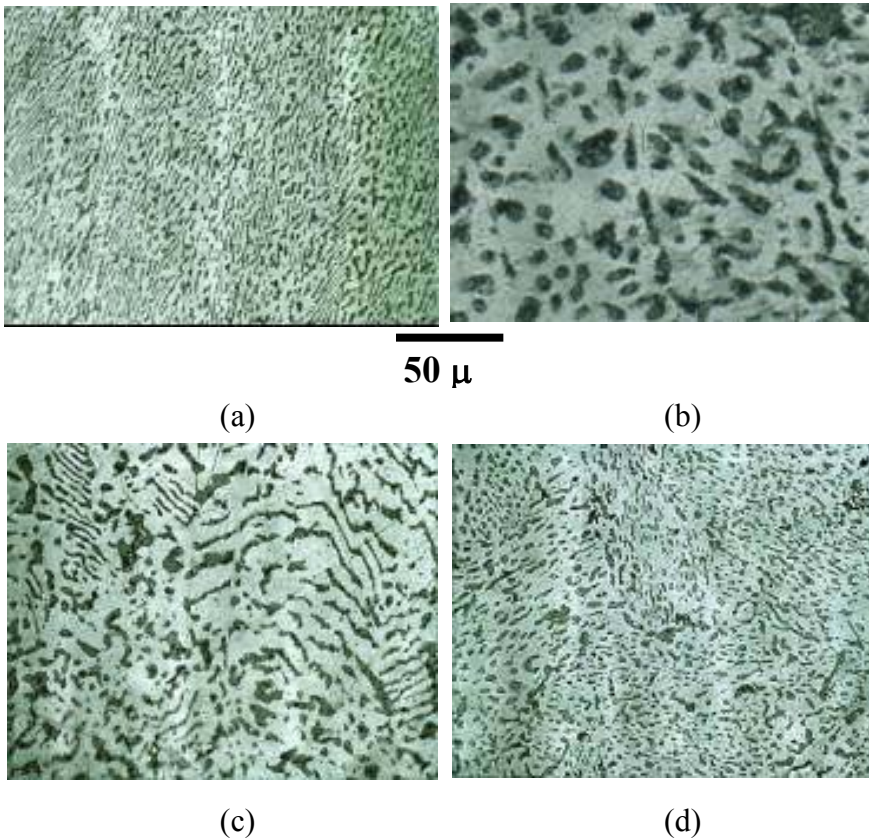


Figure 12: Microstructures of the SJS solder ball in regions close to the solder/bond-pad interface, (a) prior to thermo-mechanical cycling, and (b-d) after TMC. (b) without underfill, (c) with UF1, (d) with UF2.

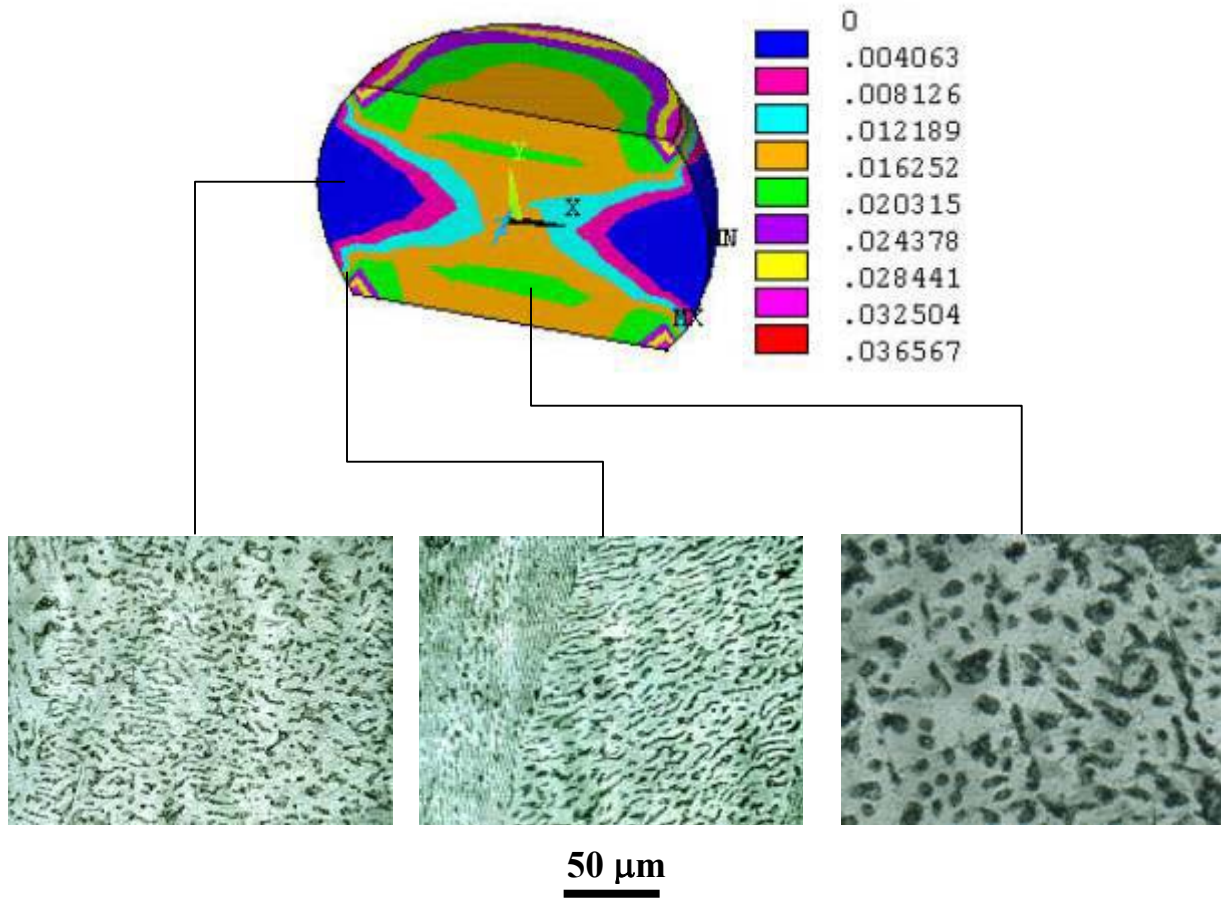


Figure 13: Distribution of equivalent effective plastic strain in an SJS solder ball without underfill following one thermal cycle. The corresponding microstructures at different locations within the solder ball after 50 thermal cycles are also shown. It is apparent that the local microstructural scale is related to the inelastic strain state.